Journal Pre-proofs

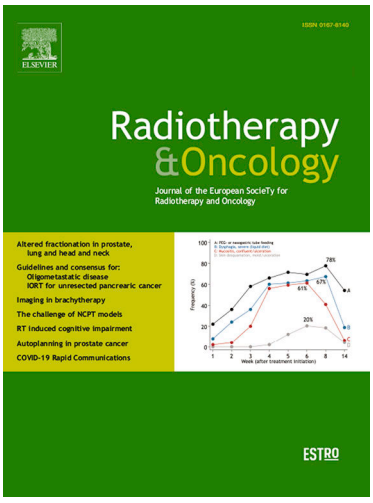

Original Article

First experimental evaluation of multi-target multileaf collimator tracking during volumetric modulated arc therapy for locally advanced prostate cancer

Emily A Hewson, Andrew Dipuglia, John Kipritidis, Yuanyuan Ge, Ricky O'Brien, Stephanie Roderick, Linda Bell, Per R Poulsen, Thomas Eade, Jeremy T Booth, Paul J Keall, Doan T Nguyen

PII: S0167-8140(21)06223-X
DOI: https://doi.org/10.1016/j.radonc.2021.05.001
Reference: RADION 8830

To appear in: *Radiotherapy and Oncology*

Received Date: 3 February 2021
Revised Date: 27 April 2021
Accepted Date: 2 May 2021

Please cite this article as: Hewson, E.A., Dipuglia, A., Kipritidis, J., Ge, Y., O'Brien, R., Roderick, S., Bell, L., Poulsen, P.R., Eade, T., Booth, J.T., Keall, P.J., Nguyen, D.T., First experimental evaluation of multi-target multileaf collimator tracking during volumetric modulated arc therapy for locally advanced prostate cancer, *Radiotherapy and Oncology* (2021), doi: https://doi.org/10.1016/j.radonc.2021.05.001

First experimental evaluation of multi-target multileaf collimator tracking during volumetric modulated arc therapy for locally advanced prostate cancer

Emily A Hewson[1*], Andrew Dipuglia[2], John Kipritidis[2], Yuanyuan Ge[3], Ricky O'Brien[1], Stephanie Roderick[2], Linda Bell[2], Per R Poulsen[4], Thomas Eade[2], Jeremy T Booth[2,5], Paul J Keall[1], Doan T Nguyen[1,2,6]

1. ACRF Image X Institute, University of Sydney School of Health Sciences, Sydney, Australia
2. Northern Sydney Cancer Centre, Royal North Shore Hospital, Sydney, Australia
3. Nelune Comprehensive Cancer Centre, Prince of Wales Hospital, Sydney, Australia
4. Department of Oncology and Danish Center for Particle Therapy, Aarhus University Hospital, Aarhus, Denmark
5. School of Physics, University of Sydney, Sydney, Australia
6. School of Biomedical Engineering, University of Technology Sydney, NSW, Australia

[*]Corresponding author at: University of Sydney, Sydney, Australia

E-mail address: emily.hewson@sydney.edu.au

Postal address:
Room 215, ATP Biomedical Building,
1 Central Avenue, Eveleigh NSW 2015

Abstract

Purpose: Locally advanced and oligometastatic cancer patients require radiotherapy treatment to multiple independently moving targets. There is no existing commercial solution that can simultaneously track and treat multiple targets. This study experimentally

implemented and evaluated a real-time multi-target tracking system for locally advanced prostate cancer.

Methods: Real-time multi-target MLC tracking was integrated with 3D x-ray image guidance on a standard linac. Three locally advanced prostate cancer treatment plans were delivered to a static lymph node phantom and dynamic prostate phantom that reproduced three prostate trajectories. Treatments were delivered using multi-target and single-target MLC tracking, and no tracking. Doses were measured using Gafchromic film placed in the dynamic and static phantoms. Dosimetric error was quantified by the 2%/2 mm gamma failure rate. Geometric error was evaluated as the misalignment between target and aperture positions. The multi-target tracking system latency was measured.

Results: The mean (range) gamma failure rates for the prostate and lymph nodes, were 18.6% (5.2%, 28.5%) and 7.5% (1.1%, 13.7%) with multi-target tracking, 7.9% (0.7%, 15.4%) and 37.8% (18.0%, 57.9%) with single-target tracking, and 38.1% (0.6%, 75.3%) and 37.2% (29%, 45.3%) without tracking. Multi-target tracking had the lowest geometric error with means and standard deviations within 0.2 ± 1.5 for the prostate and 0.0 ± 0.3 mm for the lymph nodes. The latency was 730 ± 20 ms.

Conclusion: This study presented the first experimental implementation of multi-target tracking to independently track prostate and lymph node displacement during VMAT. Multi-target tracking reduced dosimetric and geometric errors compared to single-target tracking and no tracking.

Introduction

Radiotherapy of locally advanced disease, such as prostate cancer, non-small cell lung cancer, or oligometastatic cancer, often involves multiple targets to be treated simultaneously. However, the primary tumour and associated lymph nodes can undergo large, differential motion [1-4] that compromises treatment quality [5, 6]. Evidence has supported stereotactic body radiation therapy (SBRT) as a treatment for oligometastatic cancers [7, 8], and highly accurate radiotherapy methods are essential for SBRT due to the higher doses and tighter treatment margins [9].

Despite this, there are currently no tracking methods that allow for the motion of multiple targets to be tracked independently. While real-time tracking systems such as the CyberKnife [10] and Radixact [11] are commercially available, these systems are currently not capable of adapting treatment to multiple, independent targets and require expensive specialised systems, limiting patient access to these treatments. Multileaf collimator (MLC) tracking has been developed as a real-time adaptation method that can be implemented on standard linacs [12]. To date, MLC tracking has been clinically implemented for single-target tracking to adapt to prostate [13, 14] and lung tumour motion [15].

MLC tracking is the only known adaptation method available on current clinical machines that is capable of adapting to independent motion of multiple targets. A previous study by Ge *et al*. [16] experimentally implemented multi-target MLC tracking to track single-tumour deformation and tumour-system deformation of ball phantoms on a standard linac. Liu *et al*. [17] implemented MR-guided multi-target MLC tracking on an MRI-linac to track two simultaneously moving spherical targets. As both experimental studies implemented multi-target MLC tracking for a single-field conformal treatment to track spherical targets, multi-target MLC tracking has not yet been experimentally implemented for modern clinical radiotherapy patient treatment plans. Volumetric modulated arc therapy

(VMAT) treatment plans would represent a more clinically realistic treatment scenario, however, the implementation of multi-target tracking for VMAT is more challenging due to the dynamic fields and complex aperture shapes. Following our proof-of-principle computer simulations of VMAT multi-target tracking [18], a necessary step towards the clinical realisation of this technology is the performance characterisation and experiments in a clinical setting where the delivered dose to multiple targets can be measured.

The aim of this study was to demonstrate the experimental implementation of multi-target MLC tracking on a standard linac to track a prostate phantom and lymph node phantom independently for VMAT on a standard linac in real time. The multi-target tracking method was benchmarked against methods previously used for treating locally advanced prostate cancer: single-target MLC tracking, and no tracking. As previous clinical implementations of MLC tracking have been limited to early-stage cancer, the clinical realisation of multi-target MLC tracking will expand the population of cancer patients eligible to receive MLC-adapted treatment to include locally advanced cancer and oligometastatic patients.

Methods and materials

A multi-target tracking system was implemented to deliver locally advanced prostate cancer treatment plans. The performance of the multi-target tracking system was compared to single-target tracking and no tracking based on the doses delivered and geometric accuracy using each method, as outlined in Figure 1.

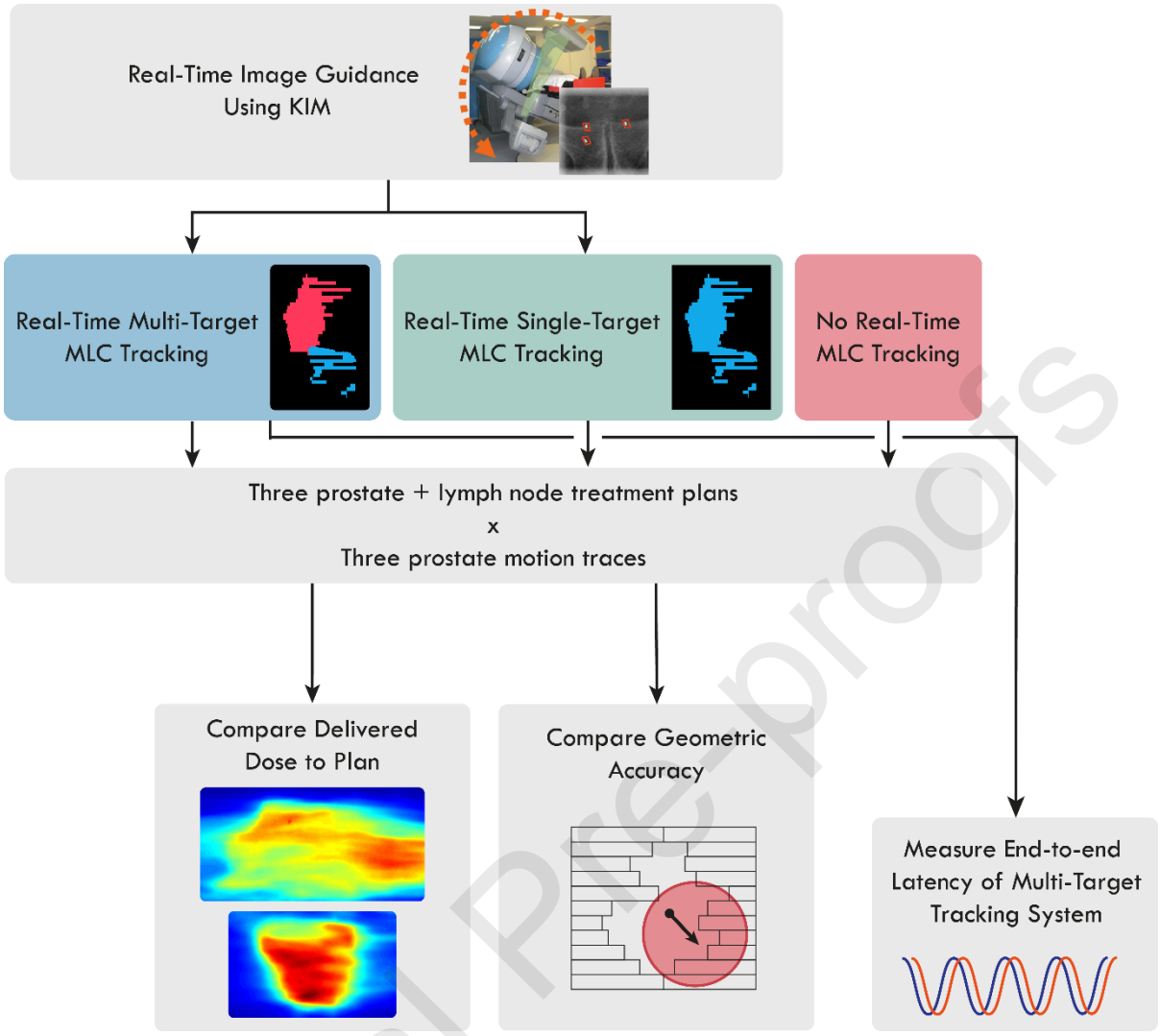

Figure 1. Kilovoltage Intrafraction Monitoring (KIM) was used to guide treatment performed using multi-target tracking, single-target tracking, or no tracking. Three locally advanced prostate cancer patient plans were delivered to a moving prostate phantom and static lymph nodes phantom. The delivered doses and geometric accuracy using each treatment method were compared. The latency of multi-target tracking was measured.

The multi-target tracking system

A multi-target tracking system was implemented on a Varian Trilogy linear accelerator (Varian Medical Systems, Palo Alto, California, United States) by combining real-time 3D image guidance using Kilovoltage Intrafraction Monitoring (KIM), and multi-target MLC tracking. The linac was equipped with a Millennium 120-leaf MLC.

KIM enables intrafraction motion monitoring to be performed on a standard linac by utilising the on-board kV imager to image the target during treatment delivery. The underlying method used by KIM can be found in [19]. KIM has previously been used with single-target MLC tracking for localised prostate cancer patients [20] with sub-mm geometric accuracy and precision for monitoring prostate motion [21]. In this study, KIM was used to monitor the motion of a moving prostate phantom with implanted fiducial markers.

The multi-target tracking algorithm implemented in this study has previously been described in a simulation study [18]. Multi-target MLC tracking was performed by first dividing the MLC apertures from the treatment plan into two sections assigned to each target prior to treatment. The field contained within the MLC aperture was discretised into a 1 mm^2 grid, and each grid element was assigned to the prostate, lymph nodes, or both, as projected in the beam's eye view (BEV) at gantry angles with 0.2° intervals. As motion was observed during treatment, the two sections of the MLC aperture were individually translated to the new positions of the targets. Finally, the deliverable MLC aperture was determined as the union of the individually translated sections with consideration of the physical leaf constraints. By combining real-time target localisation with KIM and adaptation of the radiation beam to independent targets with MLC tracking, real-time multi-target tracking was enabled on a standard linear accelerator.

Experimental setup

The multi-target MLC tracking, single-target MLC tracking [20], and no tracking methods were tested using three locally advanced prostate cancer VMAT plans that included a prostate planning target volume (PTV) and lymph node PTV. Treatment plans from three patients with varying prostate and node volumes were selected. Each patient plan was delivered to a moving phantom positioned to measure a dose plane in the prostate PTV and static phantom positioned to measure a dose plane in the lymph node PTV, shown in Figure 2. The prostate

phantom consisted of polyoxymethylene acetal with three gold fiducial markers (1 mm wide, 3 mm long) embedded. This phantom was attached to a six-degree-of-freedom (6DoF) robotic motion system that included a UR3 robot (Universal Robots, Odense, Denmark) and was programmed to reproduce patient motion traces. The robotic system was developed to allow for quality assurance of real-time adaptive radiotherapy techniques and was shown to have a static localisation accuracy within 0.09 mm in all directions, and a dynamic localisation accuracy within 0.2 mm for translation and 0.6° for rotation [22]. The prostate phantom was designed with an insertable polymethyl methacrylate (PMMA) radiochromic film holder and could be reproducibly attached to the robot arm (Figure 2b). The lymph nodes phantom was constructed using PMMA blocks that allowed for radiochromic film to be inserted (Figure 2c) and remained stationary.

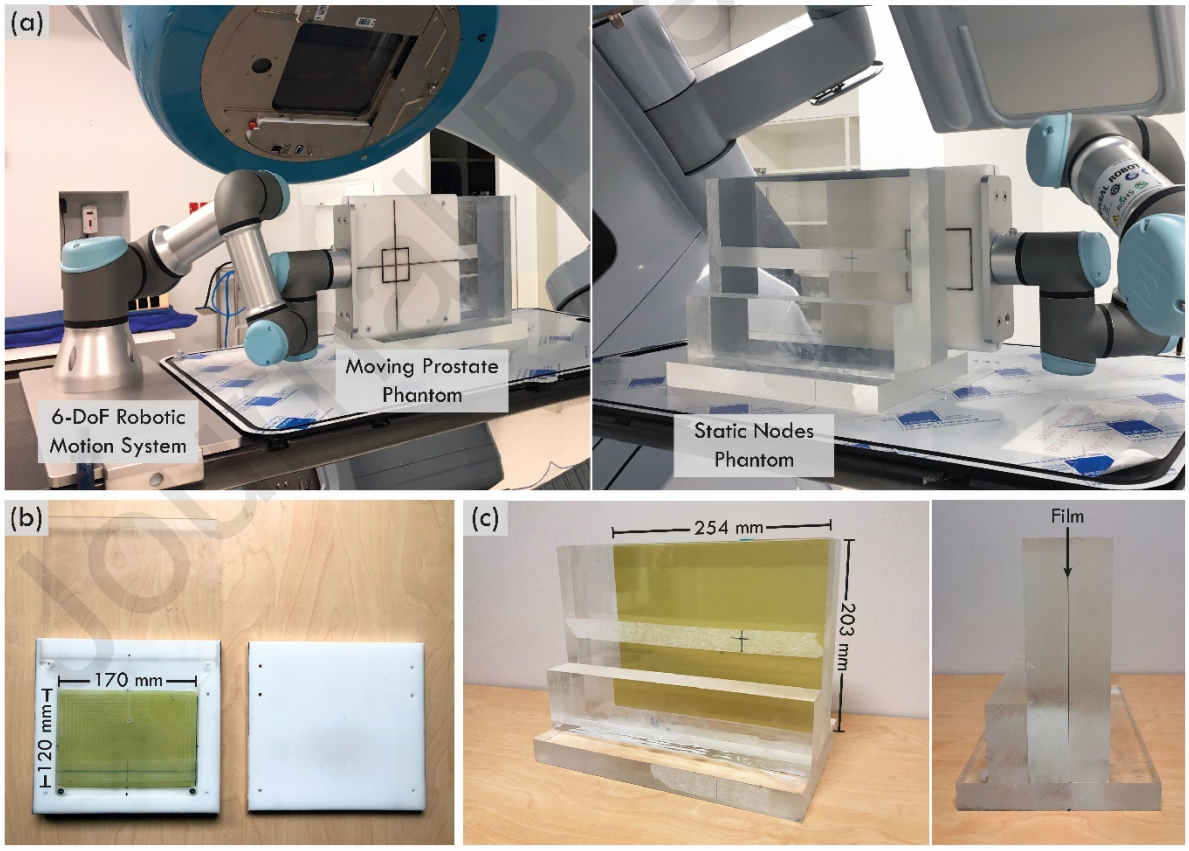

Figure 2. (a) The experimental setup used to measure dose and geometric accuracy. A six-degree-of-freedom robotic arm that held the prostate phantom, and a static nodes phantom were placed on the treatment couch. (b) Gafchromic EBT3 film was inserted in the prostate phantom. (c) A static nodes phantom was placed on the couch with a separate piece of film

inserted. The dimensions of the film used to measure the prostate and lymph node doses are indicated.

The robotic arm was programmed to reproduce three different prostate motion traces during treatment delivery. The selected motion traces are shown in Figure 3. These motion traces were selected from a database of Calypso-measured motion traces [23] to represent a range of possible motions that the prostate could undergo during treatment, including a small prostate displacement (Figure 3a), a gradual, continuous prostate drift (Figure 3b), and a large persistent prostate excursion with fast changes in displacement (Figure 3c). To demonstrate the impact of an internal interfraction prostate displacement on treatment, a shift 3 mm posterior, 2mm superior, and 2 mm right was applied at the beginning of treatment, based on root mean square deviations of prostate displacements with respect to the bony anatomy observed on MVCBCT images by Bylund *et al*. [24] This displacement was corrected using a couch shift at the beginning of treatment delivery for the single-target tracking and no tracking treatment strategies, resulting in a node displacement as shown in Figure 3. For the multi-target tracking method, the nodes phantom remained in the planned position and MLC tracking was used to correct for both the intrafraction and interfraction prostate phantom displacements.

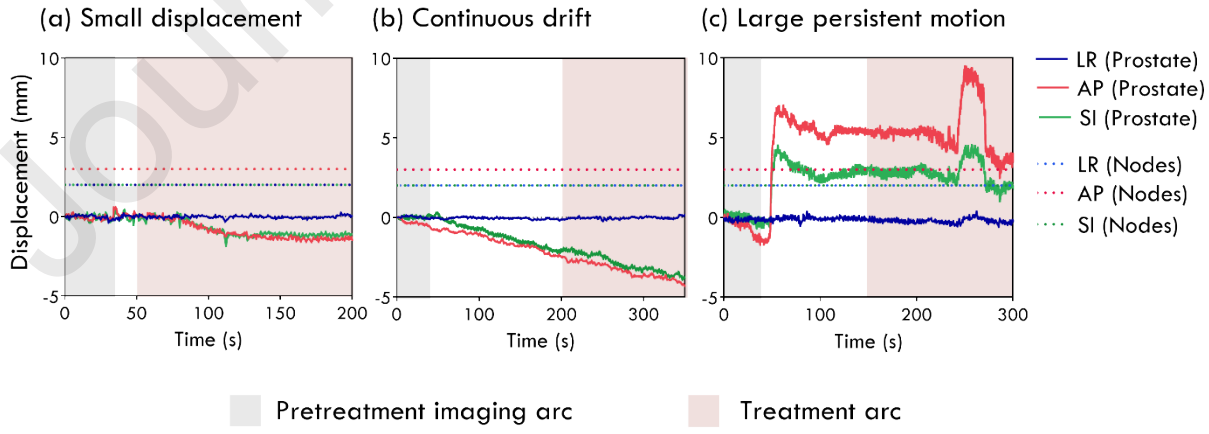

Figure 3. The prostate motion traces that were reproduced by the robotic arm. The shaded grey area indicates the motion of the prostate phantom during the pretreatment imaging arc, and the shaded red area indicates the motion during treatment delivery. The starting time of each treatment arc was chosen to capture the distinctive part of each prostate trace.

The first arc from each treatment plan was delivered with a collimator angle of 10° and gantry rotations between 181° to 179°. The monitor units (MU) for each plan were set to 1500, delivered at 600 MU/min so that the treatment time was consistent across the three treatment plans.

The prostate phantom motion was monitored in real-time using KIM. The phantom was imaged at 10 Hz and either two or three markers were segmented to monitor the motion. Multi-target MLC tracking adapted to this motion by translating the section of the aperture assigned to the prostate independently to the section assigned to the static lymph nodes. Single-target MLC tracking adapted to the prostate phantom's motion by rigidly shifting the entire MLC aperture. The MLC tracking software initiated a beam-hold if the MLC aperture motion exceeded the jaw aperture, or if excessive noise was present in the real-time target position information.

Dosimetric accuracy

The dose distributions delivered using each treatment method were measured using Gafchromic EBT3 film (Ashland, Wilmington, Delaware, United States) placed inside the prostate and node phantoms (Figure 2). Dose was measured in the sagittal plane as the prostate motion was dominant in the anterior-posterior (AP) and superior-inferior (SI) directions. Each piece of film was scanned using an Epson Expression 12000XL flatbed scanner (Seiko Epson Corporation, Nagano, Japan) with a resolution of 75 dpi before irradiation and 24 hours after irradiation.

To analyse the accuracy of dose delivery using each adaptation method, the dose delivered to the static targets in the planned position was measured to provide a reference. The doses delivered to each film with motion was compared to the reference using a 2D gamma analysis [25] with a 2% relative dose /2 mm distance-to-agreement criteria for doses

above 10% of the maximum dose in the reference film. Optical density calculations, dose calibrations, and gamma analyses were performed using the DoseLab software (version 6.80, Varian Medical Systems, Palo Alto, California, United States).

Geometric accuracy

The geometric accuracy of each treatment method was determined by computing the misalignment between the beam and the targets' positions. To calculate the geometric error, the delivered leaf positions were obtained from the treatment log files and used to create a binary image of the delivered MLC aperture. The sections of the delivered MLC aperture that were assigned to each target were compared to the binary image of the ideal MLC aperture, where each aperture section was translated to correspond to the target's motion at each time point, ignoring any physical leaf constraints. The 2D offset between the delivered and ideal MLC apertures was calculated using rigid image registration [26]. The error of the beam's position compared to the target position was computed at each point the MLC data were logged.

Latency

The end-to-end latency of the multi-target tracking system was characterised by measuring the time difference between the movement of a target and when the MLC leaves moved to the new target position. The latency was measured using the experimental set up displayed in Supplementary Figure 1a. A RANDO pelvis phantom (Radiology Support Devices, Carson, California, United States) with three gold fiducial markers implanted was placed on a HexaMotion platform (ScandiDos, Uppsala, Sweden) that was programmed to move with a sinusoidal motion (amplitude of 5 mm and periods 6 and 7.5 s) in the SI direction. A dynamic conformal treatment plan consisting of two circular apertures, to represent a moving and static target, was generated with one of the circle apertures surrounding the fiducial markers implanted in the phantom (Supplementary Figure 1b). The treatment plan was delivered to

the phantom using KIM-guidance and multi-target MLC tracking to adapt to the phantom's motion. MV images were acquired at a rate of 10 Hz during treatment delivery.

The total latency of the multi-target tracking system was calculated by measuring the time delay between the sinusoidal motion of the fiducial markers and the centre of the MLC aperture on the MV images (Supplementary Figure 1c).

Results

The gamma failure rates using 2%/2 mm pass criteria are compared in Figure 4. The overall mean gamma failure rate (Figure 4a) with multi-target tracking was 18.6% (range 5.2-28.5%) for the prostate and 7.5% (range 1.1-13.7%) for the lymph nodes. For single-target tracking, the mean gamma failure rate was 7.9% (range 0.7-15.4%) for the prostate and 37.8% (range 18.0-57.9%) for the lymph nodes. Without tracking the mean gamma failure rate was 38.1% (range 0.6-75.3%) for the prostate and 37.2% (range 29-45.3%) for the lymph nodes. The mean failure rates for each prostate motion trace are compared in Figure 4b-d.

An example of the doses delivered to film for a patient undergoing a large persistent prostate excursion (Figure 3c) and small prostate motion (Figure 3a) is shown in Figure 5a and b respectively.

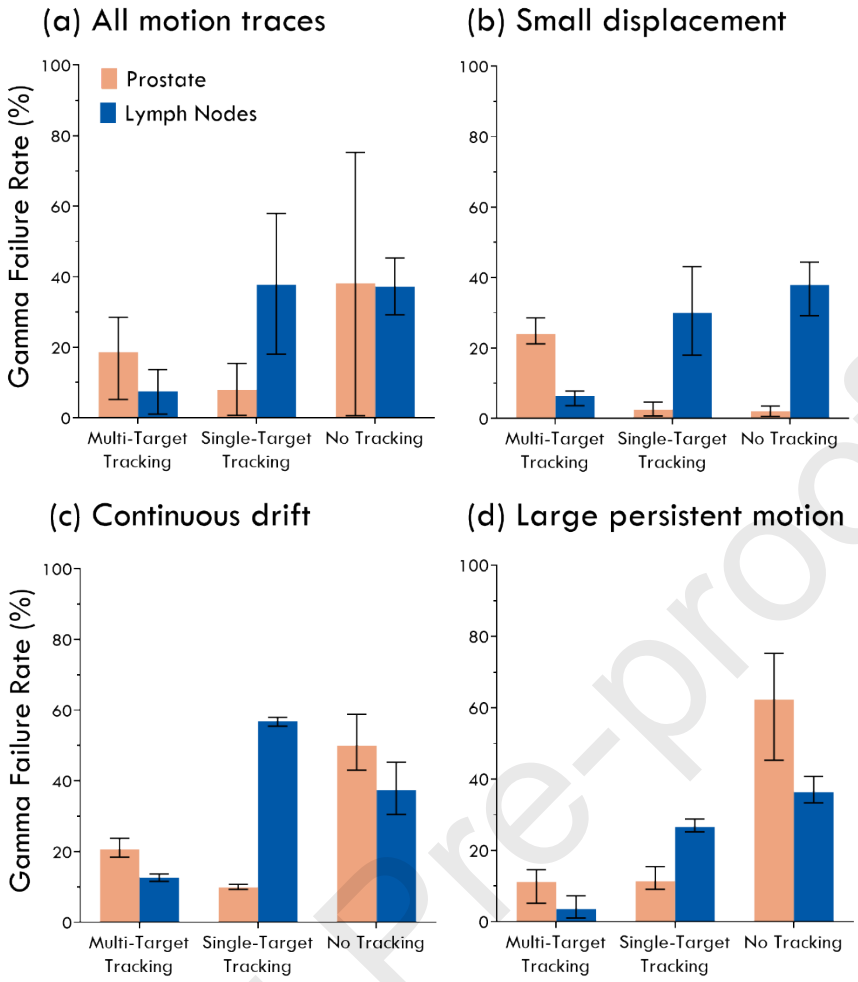

Figure 4. The motion-induced gamma failure rates with a 2%/2 mm passing criteria. (a) The mean gamma failure rates across all patient plans and motion traces. (b) The mean gamma failure rates for a small prostate displacement, (c) a continuous prostate drift, and (d) large persistent prostate motion. The error bars indicate the maximum and minimum values.

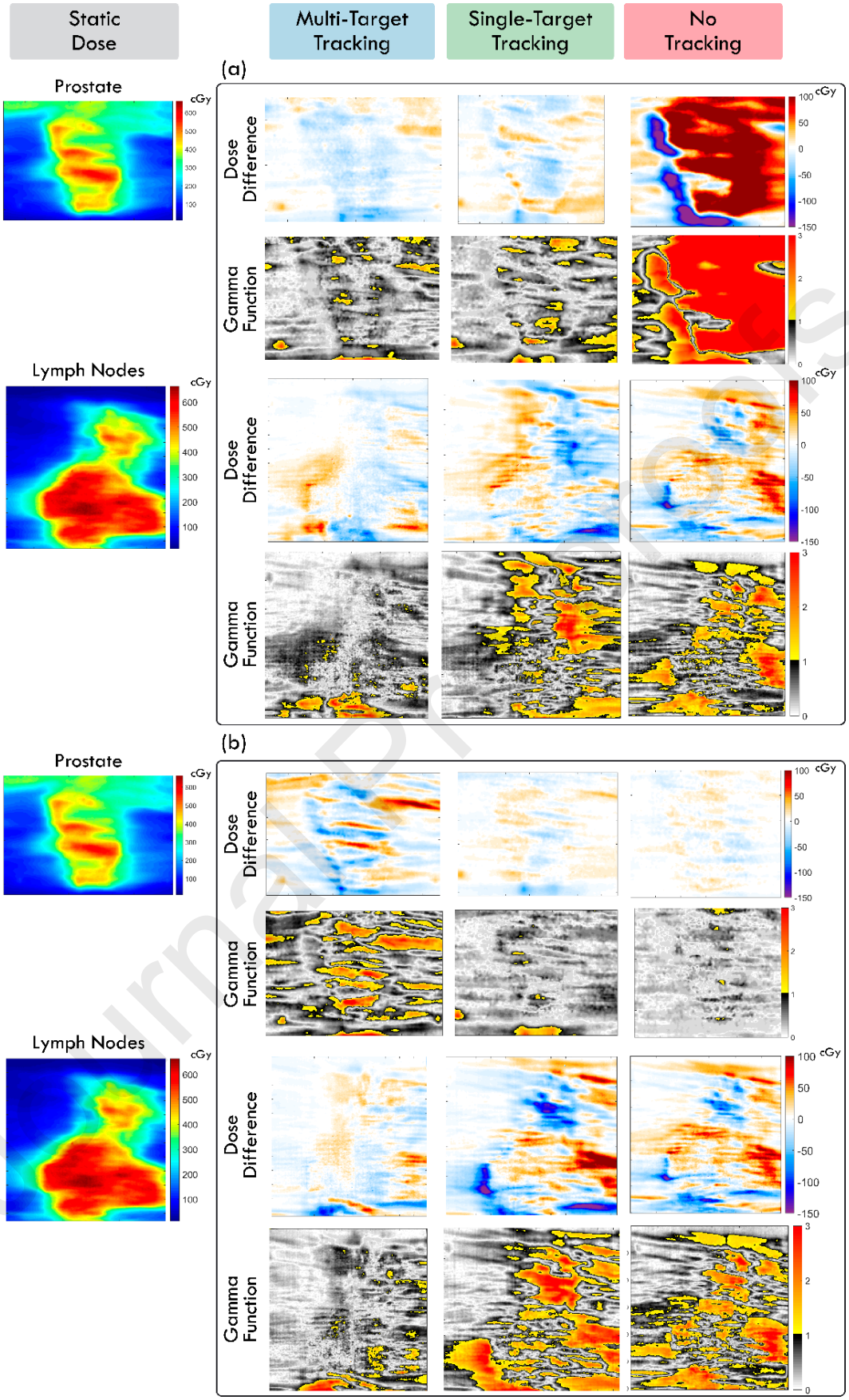

Figure 5. The planned doses delivered to film compared to the dose differences and gamma functions when using multi-target tracking, single-target tracking, or no tracking. The

example where multi-target tracking had the lowest gamma failure rate is shown in (a), and the example where multi-target tracking had the highest gamma failure rate is shown in (b).

The geometric accuracy of treatment using multi-target tracking, single-target tracking, and no tracking is plotted in Figure 6. The means and standard deviations of the geometric error are summarised in Table 1.

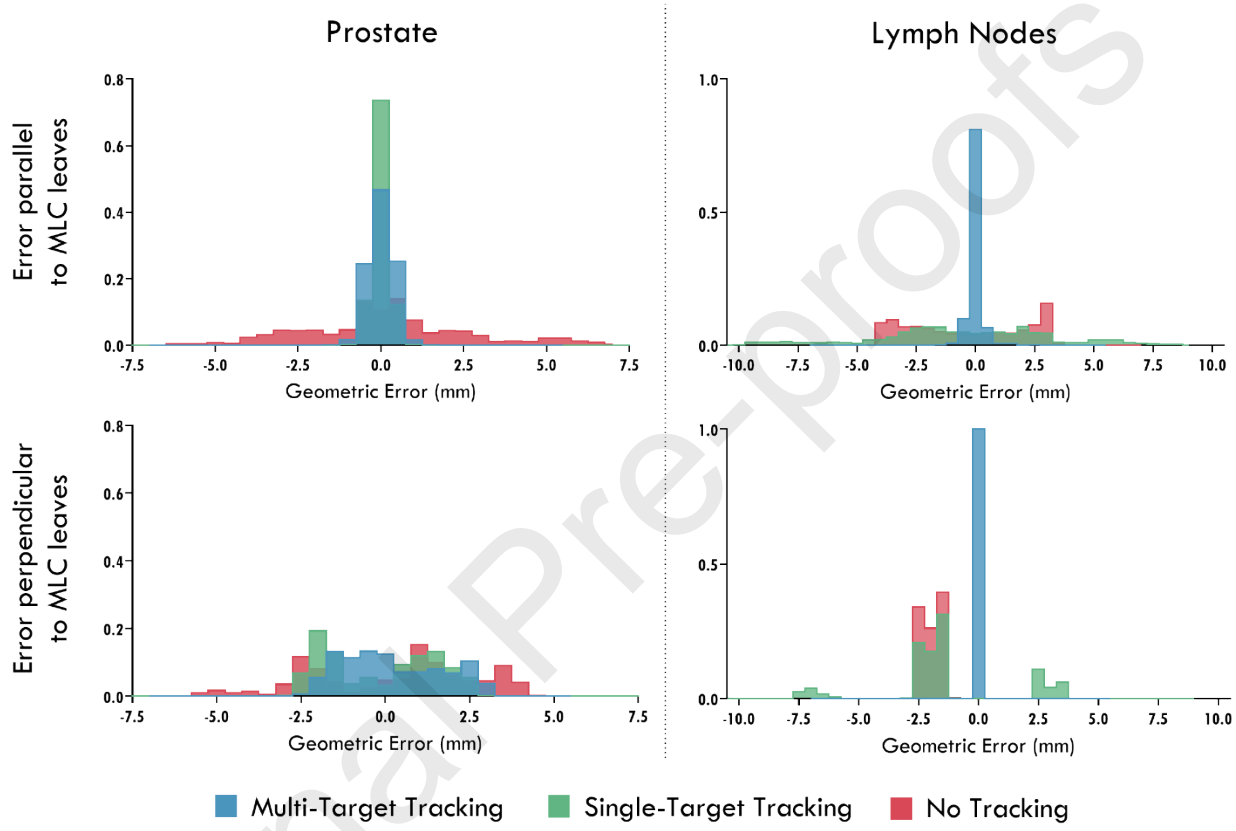

Figure 6. Distribution of geometric errors for the prostate (left) and nodes (right) with multi-target tracking, single-target tracking, and no tracking in the direction parallel (top) and perpendicular (bottom) to the MLC leaves. The data was plotted at each timestamp from the MLC logs using a bin width of 0.5 mm.

Table 1. The mean geometric error and standard deviation measured with multi-target tracking, single-target tracking and no tracking.

		Multi-Target Tracking	Single-Target Tracking	No Tracking
Prostate	Parallel to MLC leaves (mm)	0.0 ± 0.4	0.0 ± 0.2	0.2 ± 2.5
	Perpendicular to MLC leaves (mm)	0.2 ± 1.5	-0.1 ± 1.6	0.3 ± 2.4

Lymph nodes	Parallel to MLC leaves (mm)	0.0 ± 0.3	-0.5 ± 3.7	-0.4 ± 2.5
	Perpendicular to MLC leaves (mm)	0.0 ± 0.0	-1.3 ± 2.6	-2.0 ± 0.4

The mean measured latency for the multi-target tracking system was 730 ± 20 ms.

Discussion

This study demonstrated the first experimental implementation of a system that can track multiple, independently moving targets during VMAT patient plan delivery. The multi-target MLC tracking system was able to adapt the MLC aperture to the lymph node and prostate phantom displacement independently, performing adaptation in real-time using equipment available on modern standard linacs.

Multi-target MLC tracking resulted in the lowest total dosimetric error compared to single-target tracking and no tracking. The dosimetric error for the lymph nodes was lowest when using multi-target MLC tracking for all three motion traces. Larger dosimetric errors were seen for the moving prostate phantom with multi-target tracking. On average, multi-target tracking delivered a prostate dose closer to the planned dose compared to when no tracking was used. However, single-target tracking resulted in the lowest prostate dosimetric error. This came at the expense of large dosimetric errors to the nodes since single-target tracking rigidly shifted the MLC aperture to follow the prostate motion. Without tracking, dosimetric error for both targets was large as prostate motion was not tracked, and the treatment alignment to the prostate resulted in an offset for the lymph nodes.

An analysis of the treatment log files demonstrated that the multi-target tracking algorithm was able to modify the MLC aperture to track each target individually. Multi-target tracking adapted to both the prostate and node targets with submillimetre accuracy in the direction parallel to the MLC leaf motion, and with accuracy within half of the MLC leaf

width in the direction perpendicular to the MLC leaf motion. Single-target MLC tracking performed similarly to multi-target MLC tracking for the prostate, however, unsurprisingly the geometric errors were larger for the node target. When no tracking was used, the geometric error was large for both targets and was equal to the motion observed in the BEV.

The geometric error was significantly larger for motion perpendicular to the MLC leaves compared to motion parallel to the MLC leaves for both MLC tracking strategies, due to the finite leaf-width of 5 mm. The geometric error for the prostate was highest for the small prostate motion (Figure 3a) when using multi-target MLC tracking, while the persistent motion (Figure 3c) resulted in the largest error when using single-target tracking. This was likely due to the interfraction prostate displacement (3 mm posterior, 2 mm superior, and 2 mm right) and differences in initial treatment setup. Previous studies have found that the dominant source of MLC tracking error for the prostate is the limited leaf width [27]. As the multi-target tracking method was aligned to the lymph nodes phantom, the prostate phantom position in the BEV was offset with the discretisation of the MLC leaf widths during the small prostate motion, compared to single-target tracking and no tracking methods where treatment was aligned to the prostate phantom. This source of error was also reflected in the dosimetric results, where the gamma failure rate for the prostate using multi-target tracking was higher than single-target tracking, as well as no tracking for that motion trace (Figure 4b).

There were additional sources of error that could have contributed to the gamma failure rates. The treatment plans delivered in this study were created by taking the first arc from a clinical treatment plan that was originally planned with three treatment arcs. The resulting plans delivered doses that were less homogenous than the original clinical treatment plans, thus dosimetric errors due to motion were magnified. The gamma failure rates measured for single-target prostate tracking were also higher than what has been previously

measured [28]. It should also be noted that while a separate piece of film was used to measure the dose to a plane near the prostate and near the lymph nodes, there is some overlapping area between the two targets in the BEV, which would have contributed to error in the 2D gamma analysis.

The end-to-end latency of KIM-guided multi-target MLC tracking was found to be 730 ± 20 ms, which was below the threshold (1 s) set for real-time prostate tracking [29]. The latency of KIM and single-target MLC tracking have been previously measured to be 350 ms [29] and 230 ± 20 ms [30] respectively. The multi-target tracking system had a longer latency which would have contributed to the larger dosimetric and geometric errors compared to single-target tracking. The longer multi-target tracking latency was likely due to the additional computations that were required to individually calculate the new leaf positions for two separate aperture sections. While the latency was measured using a dynamic conformal arc treatment plan, the latency of the tracking system is weakly dependent on plan complexity. For prostate radiation therapy, the latency is on a smaller time scale than large changes in the target motion. Further code optimisation could reduce this latency, potentially reducing the dosimetric and geometric error of tracking. As the current multi-target optimisation engine was written as a single-threaded process, the tracking latency could be reduced by separating the aperture sections for each target and implementing a leaf-by-leaf optimisation routine using parallel computing. System latencies could be further reduced through a direct integration of KIM with the kV imaging system to eliminate the write-read delay to the hard drive.

Biological target delineation with multiparametric MRI and positron emission tomography (PSMA-PET) derived volumes for prostate cancer GTV delineation are now approaching a standard of care, giving rise to treatment with dose escalation and synchronous boosting [31]. With increased doses delivered to the target, real-time tracking of the prostate

becomes important. However, patients in this cohort may also benefit from prophylactic node irradiation. Studies measuring the setup error by comparing bony anatomy to fiducial marker position in the prostate observed up to 1 cm of differential motion in some fractions [32, 33]. Although larger PTV margins to account for this setup error may be tolerable due to lower biological doses prescribed to secondary targets, it is far from ideal. This is highlighted when considering a patient with gross nodal disease requiring a GTV node boost with a higher dose, a cohort of patients becoming more prevalent with PSMA-PET staging [34]. In these scenarios, the high dose gradient between the gross nodal disease and the small bowel will not be reproducible if also accounting for simultaneous prostate motion. With the trend toward treatments that require a higher degree of accuracy and multiple targets to be irradiated simultaneously, a method that adapts to the independent motion of multiple targets would be beneficial.

At a minimum, allowing multi-target interfraction setup would account for much of the treatment errors, with real-time tracking as the natural evolution for interfraction corrections. With the increase in the use of MRI-linacs for radiotherapy, replanning the treatment online to adapt to the patient's anatomy on the day of treatment has become an increasingly available form of treatment [35, 36]. However, prostate motion of up to 1.5cm can still be observed during treatment [23], and consequently treatment delivery accuracy will still benefit from intrafraction differential motion adaptation in addition to interfraction adaptation. Future applications in radiotherapy would ideally involve a combination of online and real-time differential adaptation, performing multi-target tracking based on the apertures optimised during the online replan.

Although prostate cancer is a suitable tumour site to test our software, clinically other disease sites may derive greater benefit. As adapting treatment to differential target displacements at setup and treatment can improve the dose to the secondary target (lymph

nodes) or reduce dose to the organs at risk (OAR) near the secondary target, other logical disease sites would include lung, oesophageal, pancreas and gynaecological cancers.

A limitation of the current study restricting its more general applicability to multi-target tracking for locally advanced and oligometastatic sites is that only the prostate target was moving and only rigid body motion was considered. As the lymph nodes are considered fixed to the pelvic vasculature [37, 38], a static phantom was appropriate to represent the nodes. Target deformation was also not considered in this study. The seminal vesicles were included with the prostate PTV for each treatment plan, however, the multi-target tracking system adapts to the prostate PTV as a rigid target despite evidence of seminal vesicle displacement relative to the prostate [39-41]. Technological advancements in MRI-linacs or ultrasound-guided radiotherapy could allow for real-time deformation tracking due to the superior soft-tissue imaging capabilities compared to x-ray imaging. MLC tracking has previously been integrated with MR- and-ultrasound guidance to track rigidly moving targets [42-45, 17] and therefore is a likely pathway for the clinical realisation of multi-target tracking.

This study has also demonstrated shortcomings of adapting to real-time motion using MLC tracking. The 5 mm MLC leaf width contributed to a large majority of the geometric error for both MLC tracking methods. Toftegaard *et al*. [46] investigated the impact of various hardware and software improvements that could potentially be made to the current MLC tracking algorithm. The strategies that were found to have the largest improvements in MLC exposure error for prostate treatments were strategies that minimised this half-leaf-width error, including rotating the collimator angle to align the leaves with the dominant target motion direction, using MLCs with a smaller leaf width, and the addition of jaw tracking. Future MLC tracking methods could also integrate with real-time dose estimation

methods [47, 48] to optimise MLC leaf positions based on accumulated 3D dose errors, as opposed to the 2D aperture fluence.

Conclusion

In this study, the implementation and experimental evaluation of MLC tracking for multiple targets for VMAT patient plans in real-time was performed for the first time. The multi-target tracking system was able to adapt two separate sections of the MLC aperture independently to track two targets with differential motion on a standard linac. Multi-target MLC tracking had the least overall dosimetric and geometric error compared to single-target MLC tracking and no tracking.

Acknowledgments

The authors acknowledge funding provided from a Cancer Council NSW Project Grant. P.J. Keall acknowledges funding from an Australian Government NHMRC Senior Principal Research Fellowship. The authors would also like to thank Dr Helen Ball, Dr Youssef Bouchta, and Dr Emily Debrot for manuscript review.

References

1. Pantarotto, J.R., A.H. Piet, A. Vincent, J.R.v.S. de Koste, and S. Senan, *Motion analysis of 100 mediastinal lymph nodes: potential pitfalls in treatment planning and adaptive strategies.* International Journal of Radiation Oncology* Biology* Physics, 2009. **74**(4): p. 1092-1099.
2. Weiss, E., S.P. Robertson, N. Mukhopadhyay, and G.D. Hugo, *Tumor, lymph node, and lymph node-to-tumor displacements over a radiotherapy series: analysis of interfraction and intrafraction variations using active breathing control (ABC) in lung cancer.* International Journal of Radiation Oncology* Biology* Physics, 2012. **82**(4): p. e639-e645.
3. Schmidt, M.L., L. Hoffmann, M.M. Knap, T.R. Rasmussen, B.H. Folkersen, J. Toftegaard, et al., *Cardiac and respiration induced motion of mediastinal lymph node targets in lung cancer patients throughout the radiotherapy treatment course.* Radiotherapy and Oncology, 2016. **121**(1): p. 52-58.
4. Kershaw, L., L. van Zadelhoff, W. Heemsbergen, F. Pos, and M. van Herk, *Image guided radiation therapy strategies for pelvic lymph node irradiation in high-risk prostate cancer: motion and margins.* International Journal of Radiation Oncology* Biology* Physics, 2018. **100**(1): p. 68-77.
5. Hwang, A., J. Chen, T. Nguyen, A. Gottschalk, M. Roach III, and J. Pouliot, *Irradiation of the prostate and pelvic lymph nodes with an adaptive algorithm.* Medical Physics, 2012. **39**(2): p. 1119-1124.
6. van Elmpt, W., M. Öllers, P. Lambin, and D. De Ruysscher, *Should patient setup in lung cancer be based on the primary tumor? An analysis of tumor coverage and normal tissue dose using repeated positron emission tomography/computed tomography imaging.* International Journal of Radiation Oncology* Biology* Physics, 2012. **82**(1): p. 379-385.
7. Creach, K.M., J.D. Bradley, P. Mahasittiwat, and C.G. Robinson, *Stereotactic body radiation therapy in the treatment of multiple primary lung cancers.* Radiotherapy and Oncology, 2012. **104**(1): p. 19-22.
8. Tree, A.C., V.S. Khoo, R.A. Eeles, M. Ahmed, D.P. Dearnaley, M.A. Hawkins, et al., *Stereotactic body radiotherapy for oligometastases.* The Lancet Oncology, 2013. **14**(1): p. e28-e37.
9. Buyyounouski, M.K., R.A. Price, E.E. Harris, R. Miller, W. Tomé, T. Schefter, et al., *Stereotactic body radiotherapy for primary management of early-stage, low-to intermediate-risk prostate cancer: report of the American Society for Therapeutic Radiology and Oncology Emerging Technology Committee.* International Journal of Radiation Oncology• Biology• Physics, 2010. **76**(5): p. 1297-1304.
10. Kilby, W., J. Dooley, G. Kuduvalli, S. Sayeh, and C. Maurer Jr, *The CyberKnife® robotic radiosurgery system in 2010.* Technology in Cancer Research & Treatment, 2010. **9**(5): p. 433-452.
11. Schnarr, E., E. Lessard, M. Beneke, D. Casey, E. Chao, J. Chappelow, et al., *Feasibility of Real-Time Motion Management on the Radixact™ System.* 2017.
12. Keall, P.J., A. Sawant, R.I. Berbeco, J.T. Booth, B. Cho, L.I. Cerviño, et al., *AAPM Task Group 264: The Safe Clinical Implementation of MLC Tracking in Radiotherapy.* Medical Physics, 2020.
13. Keall, P.J., E. Colvill, R. O'Brien, V. Caillet, T. Eade, A. Kneebone, et al., *Electromagnetic-guided MLC tracking radiation therapy for prostate cancer patients: Prospective clinical trial results.* International Journal of Radiation Oncology* Biology* Physics, 2018. **101**(2): p. 387-395.

14. Keall, P., D.T. Nguyen, R. O'Brien, E. Hewson, H. Ball, P. Poulsen, et al., *Real-Time Image-Guided Ablative Prostate Cancer Radiation Therapy: Results from the TROG 15.01 SPARK Trial.* International Journal of Radiation Oncology* Biology* Physics, 2020.
15. Booth, J., V. Caillet, A. Briggs, N. Hardcastle, G. Angelis, D. Jayamanne, et al., *MLC Tracking for Lung SABR is Feasible, Efficient and Delivers High-Precision Target dose and Lower Normal Tissue Dose.* Radiotherapy and Oncology, 2020.
16. Ge, Y., R.T. O'Brien, C.C. Shieh, J.T. Booth, and P.J. Keall, *Toward the development of intrafraction tumor deformation tracking using a dynamic multi-leaf collimator.* Medical Physics, 2014. **41**(6Part1): p. 061703.
17. Liu, P.Z., B. Dong, D. Trang Nguyen, Y. Ge, E.A. Hewson, D.E. Waddington, et al., *First Experimental Investigation of Simultaneously Tracking Two Independently Moving Targets on an MRI-Linac using Real-Time MRI and MLC Tracking.* Medical Physics, 2020.
18. Hewson, E.A., Y. Ge, R. O'Brien, S. Roderick, L. Bell, P.R. Poulsen, et al., *Adapting to the motion of multiple independent targets using multileaf collimator tracking for locally advanced prostate cancer: Proof of principle simulation study.* Medical Physics, 2021. **48**(1): p. 114-124.
19. Poulsen, P.R., B. Cho, K. Langen, P. Kupelian, and P.J. Keall, *Three-dimensional prostate position estimation with a single x-ray imager utilizing the spatial probability density.* Physics in Medicine & Biology, 2008. **53**(16): p. 4331.
20. Keall, P.J., D.T. Nguyen, R. O'Brien, V. Caillet, E. Hewson, P.R. Poulsen, et al., *The first clinical implementation of real-time image-guided adaptive radiotherapy using a standard linear accelerator.* Radiotherapy and Oncology, 2018. **127**(1): p. 6-11.
21. Hewson, E.A., D.T. Nguyen, R. O'Brien, J.H. Kim, T. Montanaro, T. Moodie, et al., *The accuracy and precision of the KIM motion monitoring system used in the multi-institutional TROG 15.01 Stereotactic Prostate Ablative Radiotherapy with KIM (SPARK) trial.* Medical Physics, 2019. **46**(11): p. 4725-4737.
22. Alnaghy, S., A. Kyme, V. Caillet, D.T. Nguyen, R. O'Brien, J.T. Booth, et al., *A six-degree-of-freedom robotic motion system for quality assurance of real-time image-guided radiotherapy.* Physics in Medicine & Biology, 2019. **64**(10): p. 105021.
23. Langen, K.M., T.R. Willoughby, S.L. Meeks, A. Santhanam, A. Cunningham, L. Levine, et al., *Observations on real-time prostate gland motion using electromagnetic tracking.* International Journal of Radiation Oncology* Biology* Physics, 2008. **71**(4): p. 1084-1090.
24. Bylund, K.C., J.E. Bayouth, M.C. Smith, A.C. Hass, S.K. Bhatia, and J.M. Buatti, *Analysis of interfraction prostate motion using megavoltage cone beam computed tomography.* International Journal of Radiation Oncology* Biology* Physics, 2008. **72**(3): p. 949-956.
25. Low, D.A., W.B. Harms, S. Mutic, and J.A. Purdy, *A technique for the quantitative evaluation of dose distributions.* Medical Physics, 1998. **25**(5): p. 656-661.
26. Guizar-Sicairos, M., S.T. Thurman, and J.R. Fienup, *Efficient subpixel image registration algorithms.* Optics letters, 2008. **33**(2): p. 156-158.
27. Poulsen, P.R., W. Fledelius, B. Cho, and P. Keall, *Image-based dynamic multileaf collimator tracking of moving targets during intensity-modulated arc therapy.* International Journal of Radiation Oncology* Biology* Physics, 2012. **83**(2): p. e265-e271.
28. Colvill, E., J. Booth, S. Nill, M. Fast, J. Bedford, U. Oelfke, et al., *A dosimetric comparison of real-time adaptive and non-adaptive radiotherapy: a multi-*

institutional study encompassing robotic, gimbaled, multileaf collimator and couch tracking. Radiotherapy and Oncology, 2016. **119**(1): p. 159-165.
29. Ng, J.A., J.T. Booth, R. O'Brien, E. Colvill, C.Y. Huang, P.R. Poulsen, et al., *Quality assurance for the clinical implementation of kilovoltage intrafraction monitoring for prostate cancer VMAT.* Medical Physics, 2014. **41**(11): p. 111712.
30. Keall, P.J., E. Colvill, R. O'Brien, J.A. Ng, P.R. Poulsen, T. Eade, et al., *The first clinical implementation of electromagnetic transponder-guided MLC tracking.* Medical Physics, 2014. **41**(2).
31. Monninkhof, E.M., J.W. Van Loon, M. van Vulpen, L.G. Kerkmeijer, F.J. Pos, K. Haustermans, et al., *Standard whole prostate gland radiotherapy with and without lesion boost in prostate cancer: Toxicity in the FLAME randomized controlled trial.* Radiotherapy and Oncology, 2018. **127**(1): p. 74-80.
32. Nederveen, A.J., H. Dehnad, U.A. van der Heide, R.J.A. van Moorselaar, P. Hofman, and J.J. Lagendijk, *Comparison of megavoltage position verification for prostate irradiation based on bony anatomy and implanted fiducials.* Radiotherapy and oncology, 2003. **68**(1): p. 81-88.
33. Johnston, M., P. Vial, K. Wiltshire, L. Bell, S. Blome, Z. Kerestes, et al., *Daily online bony correction is required for prostate patients without fiducial markers or soft-tissue imaging.* Clinical Oncology, 2011. **23**(7): p. 454-459.
34. Roach, P.J., R. Francis, L. Emmett, E. Hsiao, A. Kneebone, G. Hruby, et al., *The impact of 68Ga-PSMA PET/CT on management intent in prostate cancer: results of an Australian prospective multicenter study.* Journal of Nuclear Medicine, 2018. **59**(1): p. 82-88.
35. Raaymakers, B.W., I.M. Jürgenliemk-Schulz, G.H. Bol, M. Glitzner, A.N.T.J. Kotte, B. van Asselen, et al., *First patients treated with a 1.5 T MRI-Linac: clinical proof of concept of a high-precision, high-field MRI guided radiotherapy treatment.* Physics in Medicine & Biology, 2017. **62**(23): p. L41-L50.
36. Winkel, D., G.H. Bol, P.S. Kroon, B. van Asselen, S.S. Hackett, A.M. Werensteijn-Honingh, et al., *Adaptive radiotherapy: The Elekta Unity MR-linac concept.* Clinical and Translational Radiation Oncology, 2019. **18**: p. 54-59.
37. Shih, H.A., M. Harisinghani, A.L. Zietman, J.A. Wolfgang, M. Saksena, and R. Weissleder, *Mapping of nodal disease in locally advanced prostate cancer: rethinking the clinical target volume for pelvic nodal irradiation based on vascular rather than bony anatomy.* International Journal of Radiation Oncology* Biology* Physics, 2005. **63**(4): p. 1262-1269.
38. Lawton, C.A., J. Michalski, I. El-Naqa, M.K. Buyyounouski, W.R. Lee, C. Menard, et al., *RTOG GU radiation oncology specialists reach consensus on pelvic lymph node volumes for high-risk prostate cancer.* International Journal of Radiation Oncology* Biology* Physics, 2009. **74**(2): p. 383-387.
39. van der Wielen, G.J., T.F. Mutanga, L. Incrocci, W.J. Kirkels, E.M.V. Osorio, M.S. Hoogeman, et al., *Deformation of prostate and seminal vesicles relative to intraprostatic fiducial markers.* International Journal of Radiation Oncology* Biology* Physics, 2008. **72**(5): p. 1604-1611. e3.
40. Liang, J., Q. Wu, and D. Yan, *The role of seminal vesicle motion in target margin assessment for online image-guided radiotherapy for prostate cancer.* International Journal of Radiation Oncology* Biology* Physics, 2009. **73**(3): p. 935-943.
41. Smitsmans, M.H., J. De Bois, J.-J. Sonke, C.N. Catton, D.A. Jaffray, J.V. Lebesque, et al., *Residual seminal vesicle displacement in marker-based image-guided radiotherapy for prostate cancer and the impact on margin design.* International Journal of Radiation Oncology* Biology* Physics, 2011. **80**(2): p. 590-596.

42. Fast, M.F., T.P. O'Shea, S. Nill, U. Oelfke, and E.J. Harris, *First evaluation of the feasibility of MLC tracking using ultrasound motion estimation.* Medical Physics, 2016. **43**(8Part1): p. 4628-4633.
43. Ipsen, S., R. Bruder, R. O'Brien, P.J. Keall, A. Schweikard, and P.R. Poulsen, *Online 4D ultrasound guidance for real-time motion compensation by MLC tracking.* Medical Physics, 2016. **43**(10): p. 5695-5704.
44. Lydiard, S., V. Caillet, S. Ipsen, R. O'Brien, O. Blanck, P.R. Poulsen, et al., *Investigating multi-leaf collimator tracking in stereotactic arrhythmic radioablation (STAR) treatments for atrial fibrillation.* Physics in Medicine & Biology, 2018. **63**(19): p. 195008.
45. Glitzner, M., P. Woodhead, P. Borman, J. Lagendijk, and B. Raaymakers, *MLC-tracking performance on the Elekta unity MRI-linac.* Physics in Medicine & Biology, 2019. **64**(15): p. 15NT02.
46. Toftegaard, J., P.J. Keall, R. O'Brien, D. Ruan, F. Ernst, N. Homma, et al., *Potential improvements of lung and prostate MLC tracking investigated by treatment simulations.* Medical Physics, 2018. **45**(5): p. 2218-2229.
47. Fast, M., C. Kamerling, P. Ziegenhein, M. Menten, J. Bedford, S. Nill, et al., *Assessment of MLC tracking performance during hypofractionated prostate radiotherapy using real-time dose reconstruction.* Physics in Medicine & Biology, 2016. **61**(4): p. 1546.
48. Ravkilde, T., S. Skouboe, R. Hansen, E. Worm, and P.R. Poulsen, *First online real-time evaluation of motion-induced 4D dose errors during radiotherapy delivery.* Medical Physics, 2018. **45**(8): p. 3893-3903.

		Multi-Target Tracking	Single-Target Tracking	No Tracking
Prostate	Parallel to MLC leaves (mm)	0.0 ± 0.4	0.0 ± 0.2	0.2 ± 2.5
	Perpendicular to MLC leaves (mm)	0.2 ± 1.5	-0.1 ± 1.6	0.3 ± 2.4
Lymph nodes	Parallel to MLC leaves (mm)	0.0 ± 0.3	-0.5 ± 3.7	-0.4 ± 2.5
	Perpendicular to MLC leaves (mm)	0.0 ± 0.0	-1.3 ± 2.6	-2.0 ± 0.4